Multi-objective Optimization and Uncertainty Quantification for Inductors Based on Neural Network

Kong Xiaohan; Yin Shuli; Gong Yunyi; Igarashi Hajime

Abstract.

Purpose: The prolonged training time of the neural network (NN) has sparked considerable debate regarding their application in the field of optimization. The purpose of this article is to explore the beneficial assistance of neural network (NN)-based alternative models in inductance design, with a particular focus on multi-objective optimization and uncertainty analysis processes.

Design/methodology/approach: Under Gaussian-distributed manufacturing errors, we predict error intervals for Pareto points and select robust solutions with minimal error margins. Furthermore, we establish correlations between manufacturing errors and inductance value discrepancies, offering a practical means of determining permissible manufacturing errors tailored to varying accuracy requirements.

Findings: The NN-assisted methods are demonstrated to offer a substantial time advantage in multi-objective optimization compared to conventional approaches, particularly in scenarios where the trained neural network is repeatedly utilized. Also, NN models allow for extensive data-driven uncertainty quantification, which is challenging for traditional methods.

Originality: Three objectives including saturation current are considered in the multi-optimization, and the time advantages of the NN are thoroughly discussed by comparing scenarios involving single optimization, multiple optimizations, bi-objective optimization, and tri-objective optimization. We propose direct error interval prediction on the Pareto front, utilizing extensive data to predict the response of the Pareto front to random errors following a Gaussian distribution. This approach circumvents the compromises inherent in constrained robust optimization for inductance design and allows for a direct assessment of robustness that can be applied to account for manufacturing errors with complex distributions.

Keywords: Multi-objective optimization, surrogate optimization, uncertainties in electromagnetics.

INTRODUCTION

In the inductor design [1, 2], the introduction of a magnetic core can enhance the inductance value; however, it also introduces additional core losses. Minimizing the core losses of the inductor while achieving the desired inductance value is necessary. Another crucial optimization objective is to minimize the size of the inductor, which can reduce manufacturing costs and promote integration. Nevertheless, reducing the core volume and minimizing core losses are conflicting objectives because the reduced core volume exacerbates saturation effects, resulting in a lower saturation current. It is essential to simultaneously minimize core losses and volume while maximizing the saturation current, all while maintaining a fixed inductance value. This complex task can be addressed through multi-objective optimization [3, 4]. The objective here is to determine a Pareto front, representing the best possible trade-offs between conflicting optimization objectives. Solving a multi-objective problem necessitates significant computational effort. For instance, methods based on evolutionary algorithms require a large number of evaluations of the objective functions [5, 6]. When the performance is evaluated using finite element (FE) models, this becomes prohibitively expensive, especially when saturation current is considered. Adapting of surrogate models[7] can obviously reduce the optimization time, and neural network (NN)[8, 9] is one of the commonly used and powerful surrogate models. However, the suitability of using surrogate models for specific scenarios requires discussion: for example, the training time for surrogate models containing complex features may be substantially longer than the time for a single conventional optimization. Therefore the suitability of inductor optimization for the application of NN surrogate models still needs discussion. Previous work [10] has reported the use of the neural network (NN)-based surrogate models for multi-objective optimization of inductors, resulting in substantial speed improvements. However, this work did not consider maximizing the saturation current as an optimization objective and did not address the potential errors introduced during actual manufacturing processes.

Uncertainty quantification [11, 12] is crucial in considering the optimization, especially for precision components such as inductors. Although modern manufacturing processes have achieved high precision, it is still impossible to completely avoid the manufacturing errors. To enhance precision control, it is imperative to establish the relationship between manufacturing errors and performance errors. Based on this relationship, it becomes possible to implement machining error control in accordance with accuracy requirements. There are reports [13-15] on multi-objective optimization that take into account robustness with respect to errors. Most of the proposed algorithms advocate assessing the objective function values within a small neighbourhood and determining the robustness of a point by evaluating the disturbance level of its neighbourhood. In problems with constraint functions, the Pareto front is likely to coincide with the constraint boundaries. For problems with constraint functions (e. g. $g(x) \geq c_1$ or $g(x) \leq c_2$), it is suggested to slightly relax the constraint boundaries and select a more conservative Pareto front in the feasibility domain [15]. However, there are stringent constraints on the inductance values for the inductor design. Moving away from the boundaries to select a robust solution would cause the inductance to deviate from the target value. Consequently, robust multi-objective optimization aimed at addressing constraints is not suitable for inductor design problems. Direct evaluating the disturbance intervals of Pareto points due to manufacturing errors is another way to find robust solutions. However, this necessitates a substantial computational effort, particularly when dealing with a large number of Pareto points.Nowadays, there are some powerful methods for uncertainty quantification. For example, polynomial chaos expansion (PCE)[16] and the method of Sobol' indices[17] and Bayesian-based method[18], which has strong potential to solve the current problem. In this paper, we focus on exploring the possibility of taking advantage of the NN surrogate model to directly observe the impact of errors based on multi-objective optimization, and hopefully give an intuitive and convenient method for inductor manufacturers who care about the overall error distribution. In cases where the manufacturing error follows a specific pattern, such as a Gaussian distribution, additional sampling points become imperative to accurately approximate its distribution. The adoption of NN-based surrogate models holds the promise of substantially reducing computation time in uncertainty quantification.

In this study, the application of the NN surrogate model in multi-objective optimization and uncertainty quantification is discussed. A specific application example is given in the optimization of inductors, where the three-objective Pareto front is obtained, considering the saturation current, core loss, and core volume. The time-beneficial advantage of the NN surrogate model is illustrated by comparing optimization time with the conventional method. Furthermore, the uncertainty quantification is considered based on the Pareto front obtained. Error intervals of Pareto points are predicted based on the NN surrogate model, and points with narrow error intervals are chosen as robust points. The relationships between manufacturing errors and inductance value errors are established, which can be directly employed to determine the permissible manufacturing error in accordance with different accuracy requirements.

NN SURROGATE MODEL

The inductor model is as shown in Figure 1, and structural parameters including width (*w*), thickness (*t*) and gap length(*d*), as well as magnetic core's width (*W*) and thickness (*T*) are defined.

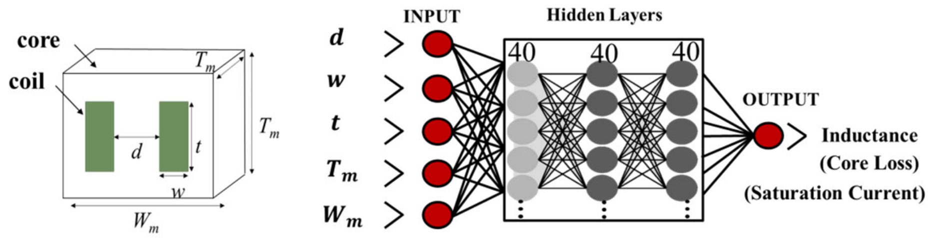

Source: Authors' own creation/work

Figure 1: Inductor model and NN structure.

Three NNs were individually trained to predict three performance characteristics: inductance, core loss, and saturation current. Figure 1 illustrates the architecture of these NNs. Each of these NNs featured three hidden layers, with the middle layer having a size of 40 neurons. The training of these NNs was conducted using TensorFlow in Python, and the NN model followed the Multilayer Perceptron (MLP) model. The training process included 500 iterations.

To train NNs for inductor optimization, we have assembled a dataset comprising 9,184 data samples. Among these, 80% of the dataset was utilized for updating the weighting coefficients, while the remaining 20% was reserved for verification purposes. The input data consists of five structural parameters, while the output data is three performance characteristics. The ranges of structural parameters are given in Table 1.

Table 1: Parameter ranges for NN training

	w	t	d	W_m	T_m
Lower Limits (mm)	**2**	**2**	**2**	**12**	**6**
Upper Limits (mm)	**20**	**20**	**20**	**50**	**30**

Source: Authors' own creation/work

Performance characteristics including the inductance, core loss and saturation current were collected by performing finite element (FE) calculation. As shown in Figure 2(a), we simplified the inductor calculation model into a two-dimensional (2-D) quarter one. The B-H curve of the core material is given in Figure 2(b).The definition of saturation current refers to the current passing through the winding when the inductance decreases to 70% of its standard value. It's worth noting that the saturation current value requires multiple iterative calculations. The settings for FE calculation are given in Table 2. For simplicity, we assume that the current in the inductor is directly proportional to the cross-sectional area of the wire, and the current density per unit area is set to 2500 A/m^2.

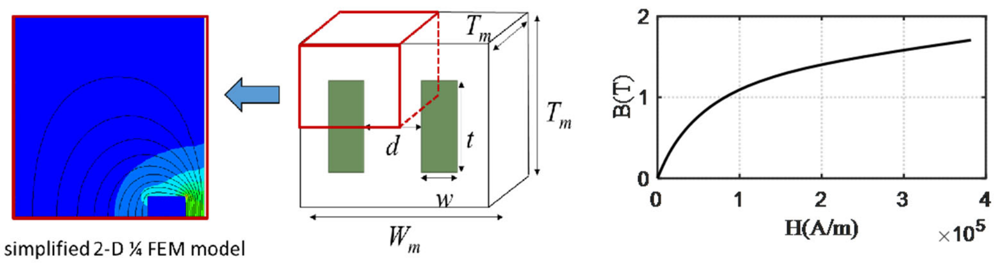

(a) (b)

Source: Authors' own creation/work

Figure 2 Indutor model. (a) Calculation model for the inductor, and (b) B–H curve of the core.

Table 2: Parameters for FEM calculation

	Current density (A/m^2)	*Frequency* (Hz)	*Core loss* ($W=K_hB^{\alpha}f^{\beta}$)		
			K_h	α	β
Parameters	**2500**	**100000**	**211.19**	**1.688**	**1.219**

Source: Authors' own creation/work

Figure 3 shows the comparison of results between the 2-D and 3-D models, where the 3-D model has a closed coil loop. Sixty-five structures were randomly selected within the size range of Table 1, and their calculated results are scattered in ascending order respectively. Although there are some discrepancies, the 2-D model based results still expresses the correct data trend. The average calculation time of a single 3-D FEM model is about 4 min, while the 2-D FEM model is about 18 s. The following analysis is based on 2-D models, but the reader can easily apply the method to 3-D models if greater accuracy is required.

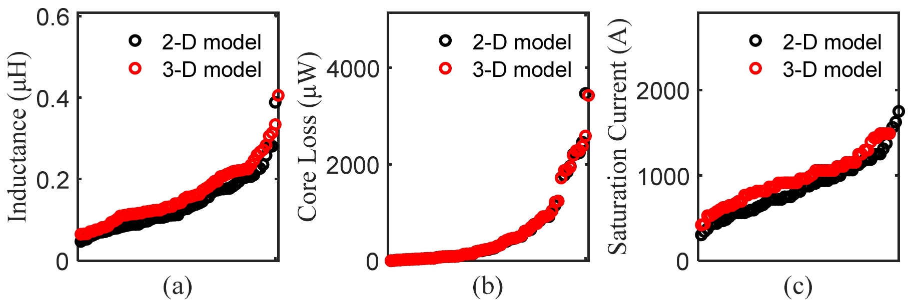

Source: Authors' own creation/work

Figure 3 Comparison between 2-D and 3-D models. (a) Inductance, (b) core loss, and (c) saturation current.

More training data leads to higher prediction accuracy, as we all know. Figure 4 shows the selection process of number of training data. Consistent with common sense, the coefficient of determinations (R^2) increases with the increased size of the training dataset. Finally, the size of the training dataset was set to be 9184 , and the estimated time needed to gather data is approximately 46 hours.

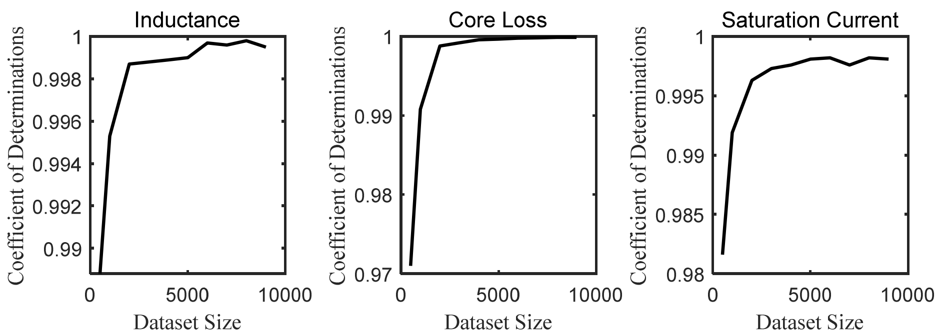

Source: Authors' own creation/work

Figure 4 The coefficient of determinations (R^2) increases with the size of the training dataset.

Training NNs using this dataset can be accomplished in just under 1 minute. Consequently, the total training time for the NNs sums up to 46 hours. Figure 5 shows the regression analysis on simulation results and NN prediction results, which indicates that both the R^2 is more than 0.998.

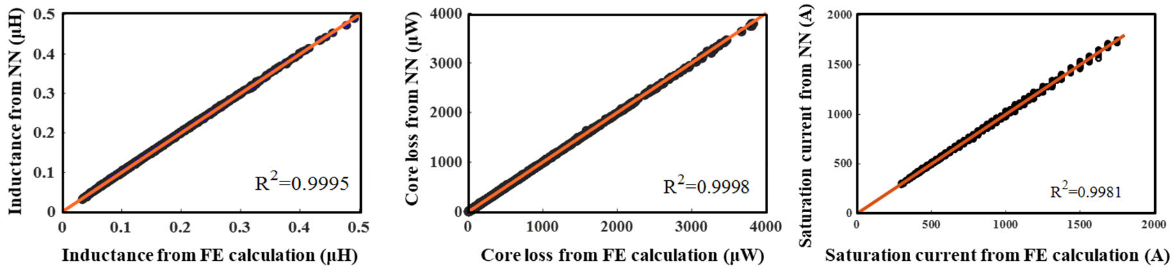

Source: Authors' own creation/work

Figure 5: Regression analysis on FE calculation and NN prediction results.

MULTI-OBJECTIVE OPTIMIZATION

In the design of inductors, there are often multiple design requirements. The primary design requirement is, of course, the value of the inductance. In addition to this, designers aim for lower core losses, smaller core volume, and a higher saturation current. However, the latter three design requirements often exhibit a competitive nature. When the core volume is reduced, the core is more prone to reaching saturation, resulting in larger core losses and a smaller saturation current. This is a constrained multi-objective problem (MOP) where, under the given constraint on inductance values, there is no single solution that is optimal in all three other characteristics. NSGA-II (Non-dominated Sorting Genetic Algorithm II) is used to address this problem, aiming to find the Pareto front within the specified inductance values.

First, let's define this MOP. The design variables are the structural parameters given in Figure 1(a). We have defined five structural parameters. To keep the design within a reasonable range, we set the coil cross-sectional area as a constant value of 40 mm^2. Therefore, the five structural parameters are reduced to four, namely, d, w, T_m, and W_m. Additionally, there is a relationship between t and w as

$$t = 40 \ mm^2/w \tag{1}$$

Then, we define the MOP as:

$$\boldsymbol{x} = [d, w, T_m, W_m], \tag{2}$$

$$F(\boldsymbol{x}) = (f_1(\boldsymbol{x}), f_2(\boldsymbol{x}), -f_3(\boldsymbol{x})), \tag{3}$$

$$\text{with } g(\boldsymbol{x}) \geq L_0, \tag{4}$$

where f_1, f_2 and f_3 represent for core loss, core volume and saturation current, respectively.

During the optimization process, it necessitates multiple evaluations of various performance characteristics of the inductor. In traditional methods, each performance evaluation is accomplished through FE calculation, which can be time-consuming. In this study, the performance evaluation of the inductor can be expedited by employing pre-trained NNs, nearly achieving instantaneous results and significantly reducing the optimization time. To be more specific, the inductance, core loss, and saturation current are all predicted using three pre-trained NNs, while the core volume can be directly computed from the structural parameters of the inductor.

First, we consider a two-performance case. Only saturation current and core volume are considered in the optimization. A total of 10,000 performance evaluations are required in one optimization. With traditional methods, this would take approximately 50 h, whereas when using NN prediction, it only takes about 16 s. Of course, we must also take into account the training time of the NN. With the use of the NN surrogate model, the cumulative optimization time is 46 h 16 s. Compared to the duration of the traditional method of 50 hours, it may seem that the NN approach does not provide a significant time advantage. In practice, however, a well-trained NNN can be used iteratively to optimize across multiple scenarios. The field of inductor design serves as an exemplary case.

The intricate variety of electronic circuits generates a multitude of different inductor design requirements, often requiring the creation of thousands of inductor values within a single product series. In scenarios where multiple designs are required, the NN-based approach undoubtedly provides a distinct time advantage. To illustrate this perspective, we performed 11 MOPs, each with different inductor values as design constraints. The resulting optimization results are shown in Figure 6.

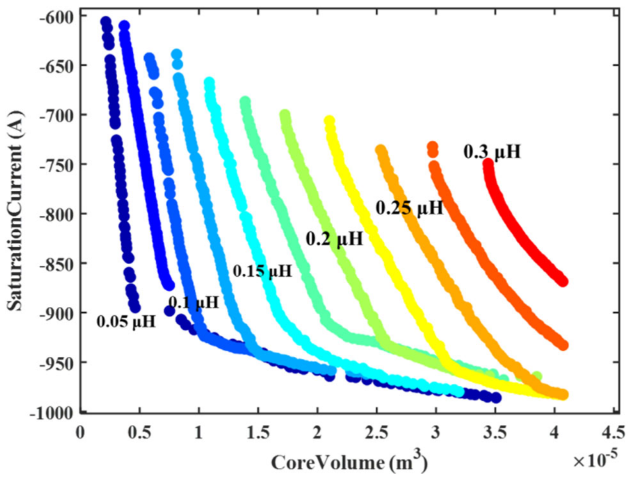

Source: Authors' own creation/work

Figure 6: Pareto fronts considering saturation current and core volume, when required inductance L_0 is (0.05, 0.075, 0.10, 0.125, 0.15, 0.175, 0.20, 0.225, 0.25, 0.275, 0.30) μH*, respectively.*

To gain deeper insights into the interplay among multiple design requirements in inductor design, we conducted multi-objective optimization for three performance parameters of a specified inductor. As depicted in Figure 7, these three performance parameters, including core loss, core volume, and saturation current, exhibit competitiveness and form a Pareto front in the three-dimensional objective function space.

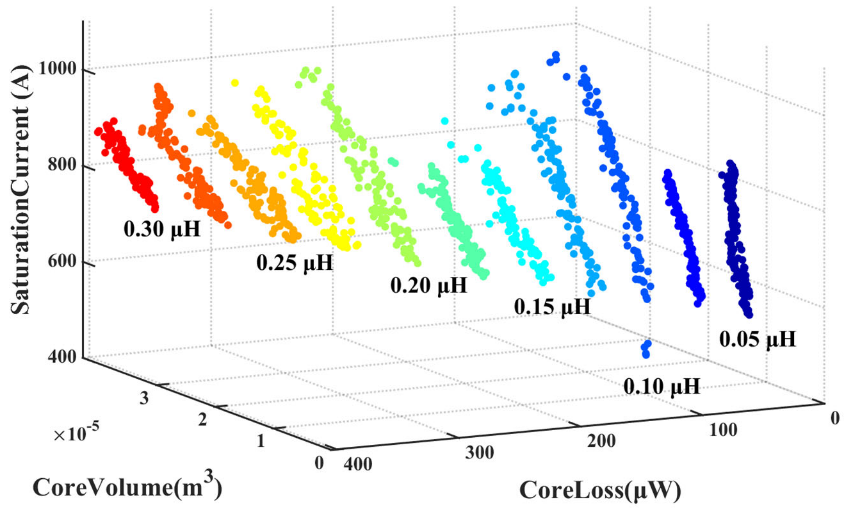

Source: Authors' own creation/work

Figure 7: Pareto fronts considering core loss, core volume and saturation current, when required inductance L_0 is (0.05, 0.075, 0.10, 0.125, 0.15, 0.175, 0.20, 0.225, 0.25, 0.275, 0.30) µH, *respectively.*

For the sake of a straightforward comparison, both in single and multiple optimization scenarios, we have depicted the time comparison between the NN-based approach and the traditional method in Figure 8. From the graph, it is evident that the total optimization time in the NN-based optimization is primarily dictated by the time required for NN training. The optimization time is minimal and almost negligible. In contrast, the traditional method's principal time expenditure arises from the repetitive evaluation using FE calculation, resulting in a linear increase in total optimization time with the number of optimizations. Take the case "11 times of optimization with two objectives" for example, the overall time is 46.05 h, including 46 h of NN training time and 0.05 h of optimization time. In contrast, the conventional method takes 550 h, all of which is optimization time. Naturally, as the number of optimizations increases, the time advantage of the NN-based approach becomes increasingly pronounced. This underscores that the NN-based approach is particularly well-suited for scenarios where the same model needs to be employed for multiple optimizations with varying design requirements.

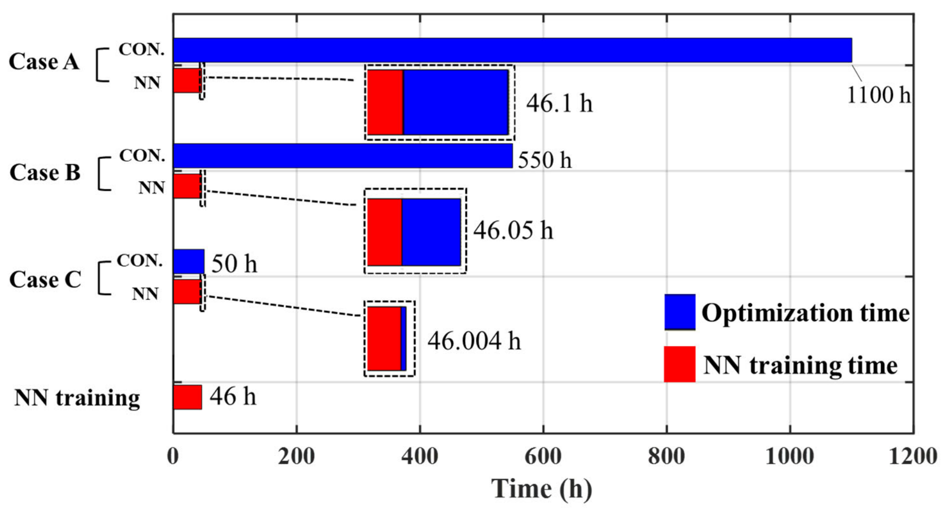

Source: Authors' own creation/work

Figure 8: Time comparison in single and multiple optimization scenarios.

Notes: Case A: 11 times of optimization with three objectives;

Case B: 11 times of optimization with two objectives;

Case C: Single optimization.

UNCERTAINTY QUANTIFICATION

Uncertainty quantification is crucial in practical manufacturing because it can provide guidance for allowable errors in the fabrication process. Therefore, observing the responses of points on the Pareto front to manufacturing errors provides an intuitive measure of the robustness of each point to disturbances. Additionally, as the inductance value inherently stands as the paramount characteristic in inductance manufacturing, through uncertainty quantification we can establish the relationship between inductance value errors and manufacturing errors. As a result, this process helps establish precise error control limits that are crucial for attaining the desired levels of inductance accuracy.

Since actual manufacturing errors often follow a random distribution, we employ a Gaussian distribution model to simulate their distributions. As shown in the Figure 9, we introduce Gaussian random perturbations to four structural parameters. Based on the Pareto front when the inductance value is 0.2 μH, we can observe the responses of all dominant points. In this chapter, we adopt the two-objective Pareto fronts considering core loss and core volume.

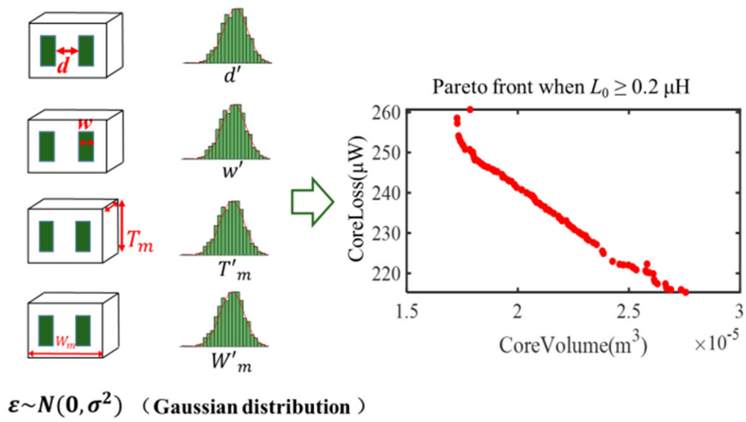

Source: Authors' own creation/work

Figure 9: Gaussian-distributed perturbations were added to four structural parameters to observe the response of the Pareto front.

Figure 10 illustrates the response of the Pareto front at various disturbance levels. The four different disturbance levels correspond to Gaussian distribution standard deviations σ of 0.0001, 0.0005, 0.001, and 0.003, respectively. In order to standardize the level of error across various dimensions, we employed normalized value to represent the Gaussian distribution standard deviation of the error σ, which depends on the value of upper and lower limits given in Table 1. For instance, in the case of dimensions w and W_m, when σ is set to 0.0001, they correspond to 0.0018 mm (calculated as 0.0001 times (20-2) mm) and 0.0038 mm (calculated as 0.0001 times (50-12) mm), respectively. The green plots above each Pareto front image represent the probability density functions for each standard deviation. At different disturbance levels, the Pareto front exhibits varying degrees of dispersion, defined as the distance away from the original dominant position. The colour bar associated with each grey point represents the inductance value. From Figure 10, it can be observed that as the Gaussian distribution standard deviation increases, the degree of dispersion of dominant points in the Pareto front increases, indicating a more pronounced deviation from the optimal position. At the same disturbance level, variations in the degree of dispersion among dominant points can be observed. Taking Figure 10 (d) as an example, the points in region A exhibit significantly less dispersion than those in region B, suggesting better robustness to manufacturing in that area.

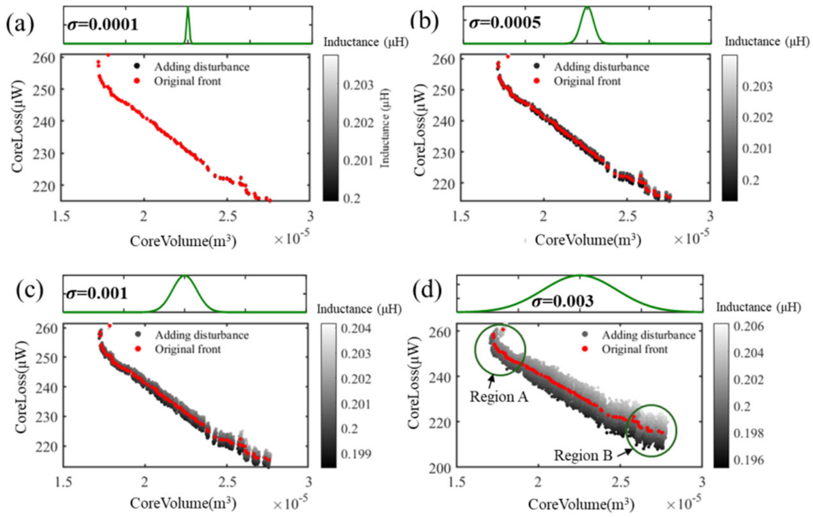

Source: Authors' own creation/work

Figure 10: Responses of the Pareto front after adding different levels of disturbances on structural parameters, where σ is the normalized value of Gaussian distribution standard deviation.

Notes: The corresponding standard deviation of real sizes are as follows: (a) w, t, d = 0.0018 mm, W_m= 0.0038 mm , T_m=0.0024 mm; (a) w, t, d = 0.009 mm, W_m= 0.019 mm , T_m=0.012 mm; (a) w, t, d = 0.018 mm, W_m= 0.038 mm , T_m=0.024 mm; (a) w, t, d = 0.054 mm, W_m= 0.114 mm , T_m=0.072 mm.

Furthermore, we conducted an analysis of the response of inductance values to manufacturing error disturbances, as depicted in Figure 11. In the original Pareto front, all dominant points had an inductance value of 0.2 μH. Upon introducing disturbances, the inductance values of these dominant points also exhibited a Gaussian distribution. As the standard deviation of manufacturing errors gradually increased, the distribution of inductance values became more dispersed. Based on the requirements for inductance error, we can establish corresponding size error control ranges.

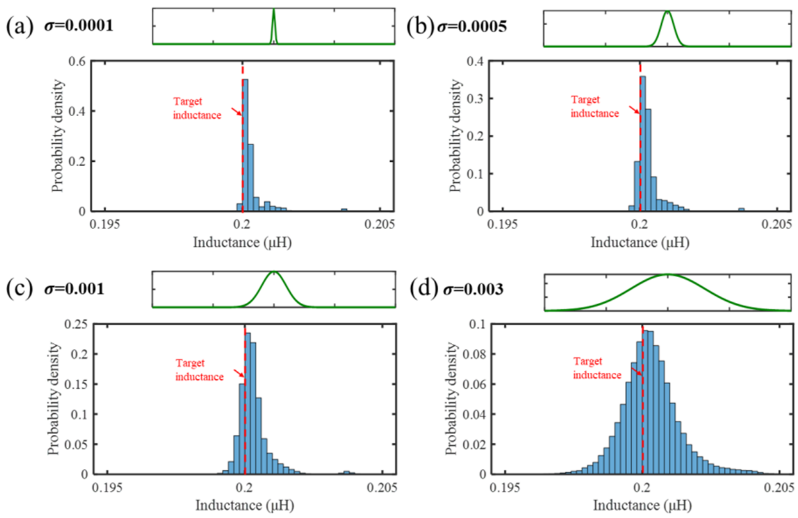

Source: Authors' own creation/work

Figure 11: Responses of the inductance after adding different levels of disturbances on structural parameters.

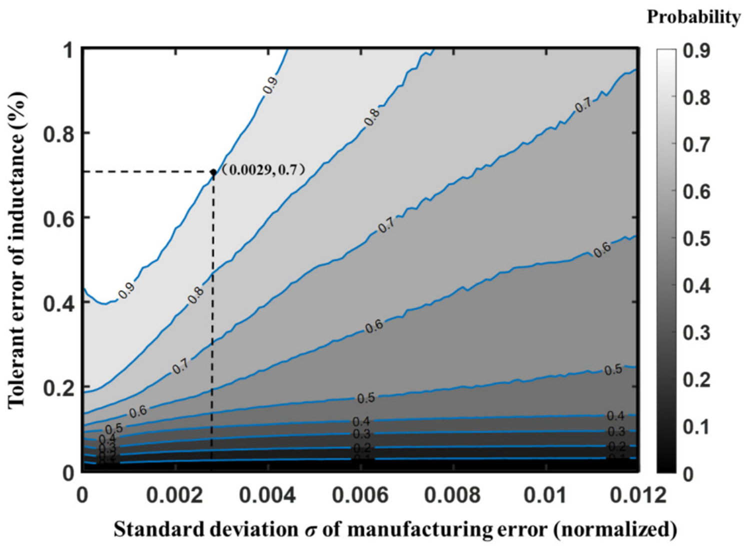

Source: Authors' own creation/work

Figure 12: Tolerance error of inductance with standard deviation σ of structural size.

By analysing the distribution of inductance values and the distribution of machining errors, we can determine the maximum allowable machining error corresponding to the design requirements for the inductance (e.g., tolerance errors of 0.2 %, 0.4 %, 0.6 %, 0.8 %, and 1 %). In Figure 12, the horizontal axis represents the standard deviation of the Gaussian distribution of machining errors, with a smaller standard deviation indicating higher machining precision. The vertical axis represents the error between actual inductance values and the standard value. This figure is generated by contour lines, where the contour values represent the probability. To illustrate this, we consider a point as an example: in order to have a 90% confidence level that the error in inductance values is within 0.7 %, corresponding to the 0.7 % scale on the vertical axis, one can locate the point on the 0.9 contour line, which leads to a maximum allowable machining error with a normalized standard deviation of 0.0029. Following this rule, we provide the corresponding data in Table 3.

Table 3: Inductance error and manufacturing error

Tolerance error of inductance	*Probability*	*Standard deviation σ of manufacturing error (normalized)*
± 0.2 %	**0.9**	**------**
	0.8	**0.0004**
	0.7	**0.0015**
± 0.4 %	**0.9**	**0.0005**
	0.8	**0.0024**
	0.7	**0.0040**
± 0.6 %	**0.9**	**0.0022**
	0.8	**0.0041**
	0.7	**0.0069**
± 0.8 %	**0.9**	**0.0034**
	0.8	**0.0060**
	0.7	**0.0099**

Source: Authors' own creation/work

We also analysed the individual impacts of each structural parameter on the design outcomes to facilitate the adoption of different error control standards during machining. We separately introduced Gaussian distribution errors to each of the four parameters. The influence of these four parameters on the Pareto front can be observed in Figure 13 when all four parameters have a normalized standard deviation of 0.001. In this example, the perturbation levels caused by the four parameters on the Pareto front are quite similar, with no significant distinctions.

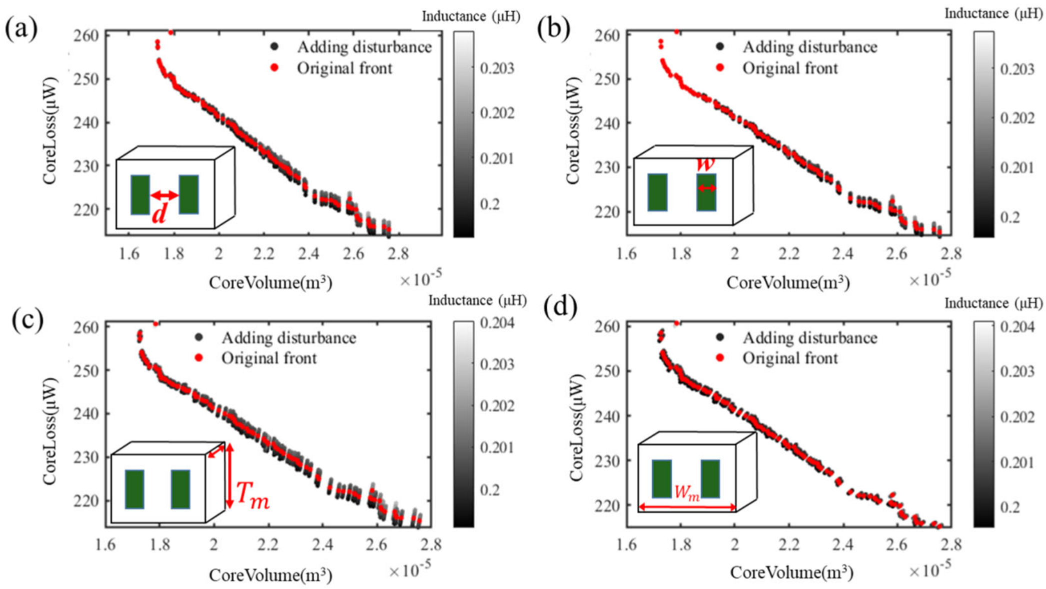

Source: Authors' own creation/work

Figure 13: Responses of the Pareto front when disturbances to different structural parameters are added separately.

Furthermore, the effects of perturbations in individual structural parameters on the inductance are presented in Figure 14. Based on the error responses of inductance to different structural parameters, varying error control standards can be specified.

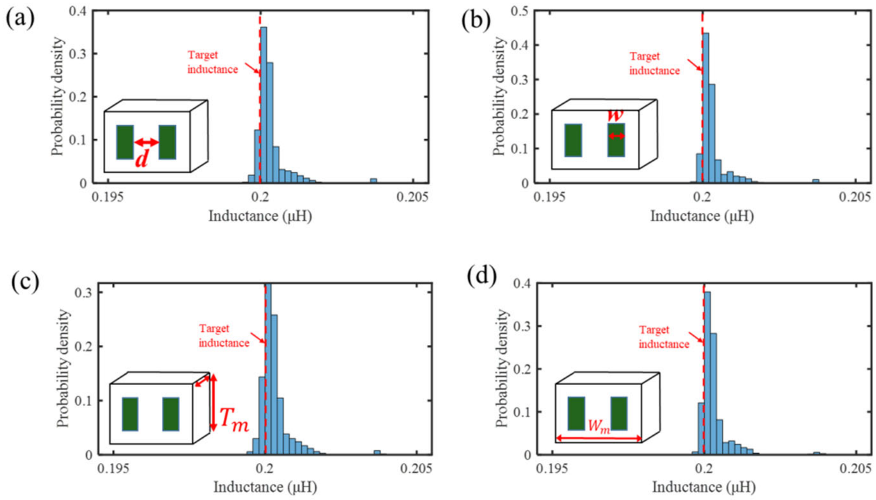

Source: Authors' own creation/work

Figure 14: Responses of the inductance when disturbances to different structural parameters are added separately.

CONCLUSIONS

In this work, the NN-based surrogate model was used for the design of inductors, which obviously accelerated the process of multi-objective optimization. The time-beneficial advantage of the NN surrogate model was discussed by comparing the optimization time with the conventional method, which is particularly obvious when there is a large number of design needs. The uncertainty quantification of optimized Pareto front was also carried out based on the NN surrogate model. The robust solution can be selected by comparing the disturbance levels of Pareto points due to manufacturing errors directly. Furthermore, the direct relationships between fabrication tolerance errors and inductance value errors were established, from which the guidance for manufacturing error can be obtained. This NN-based surrogate model can be expanded to the design of other electronic circuits such as capacitors and resistors, or some electromagnetic devices such as wireless power transfer coils and radio frequency coils.

REFERENCES

[1] Y. Sato, K. Kawano and H. Igarashi(2022), "Direct Inverse Modeling for Electromagnetic Components Using Gaussian Kernel Regression", *IEEE Transactions on Magnetics*, Vol.58, No.5, pp.1-8, doi: 10.1109/TMAG.2022.3152024.

[2] T. Sato, S. Aya, H. Igarashi, M. Suzuki, Y. Iwasaki, and K. Kawano(2015), "Loss computation of soft magnetic composite inductors based on interpolated scalar magnetic property", *IEEE Transactions on Magnetics*, Nol.51, No.3, pp.1-4, doi: 10.1109/TMAG.2014.2359983.

[3] K. Deb, A. Pratap, S. Agarwal and T. Meyarivan(2002), "A fast and elitist multiobjective genetic algorithm: NSGA-II", *IEEE Transactions on Evolutionary Computation*, Vol. 6, No. 2, pp. 182-197, doi: 10.1109/4235.996017.

[4] F. Campelo, F. G. Guimaraes and H. Igarashi(2008), "Multiobjective Optimization Using Compromise Programming and an Immune Algorithm", *IEEE Transactions on Magnetics*, Vol. 44, No. 6, pp. 982-985, doi: 10.1109/TMAG.2007.916354.

[5] S. Koziel, P. Kurgan and J. W. Bandler (2017), "Multi-objective mixed-integer design optimization of planar inductors using surrogate modeling techniques", *2017 IEEE MTT-S International Microwave Symposium (IMS), Honolulu, HI, USA,* pp. 1632-1634, doi: 10.1109/MWSYM.2017.8058950.

[6] R. González-Echevarría et al.(2014), "Automated Generation of the Optimal Performance Trade-Offs of Integrated Inductors," *IEEE Transactions on Computer-Aided Design of Integrated Circuits and Systems*, Vol. 33, No. 8, pp. 1269-1273, doi: 10.1109/TCAD.2014.2316092.

[7] lizadeh, R., Allen, J.K. and Mistree(2020), "F. Managing computational complexity using surrogate models: a critical review", *Research in Engineering Design*, Vol.31, pp.275–298, doi: 10.1007/s00163-020-00336-7

[8] H. Sasaki and H. Igarashi(2019), "Topology Optimization Accelerated by Deep Learning," *IEEE Transactions on Magnetics*, Vol. 55, No. 6, pp. 1-5, doi: 10.1109/TMAG.2019.2901906.

[9] Pawłowski, J., Kutorasiński, K. & Szewczyk, M. Multifrequency(2022), "Nonlinear model of magnetic material with artificial intelligence optimization", *Scientific Reports,* Vol.12, No.1, pp.19784. doi: 10.1038/s41598-022-23810-9.

[10] S. Doi, H. Sasaki and H. Igarashi(2019), "Multi-Objective Topology Optimization of Rotating Machines Using Deep Learning," *IEEE Transactions on Magnetics*, Vol. 55, No. 6, pp. 1-5,doi: 10.1109/TMAG.2019.2899934.

[11] Gawlikowski, Jakob et al (2021). "A survey of uncertainty in deep NNs." *Artificial Intelligence Review,* Vol.56, pp.1513 - 1589, doi: 10.48550/arXiv.2107.03342.

[12] Moloud Abdar et al(2021). "A review of uncertainty quantification in deep learning: Techniques, applications and challenges", *Information Fusion*, Vol. 76, pp. 243-297, doi: 10.1016/j.inffus.2021.05.008.

[13] E. Gord, R. Dashti, M. Najafi, M. Tahavori and H. R. Shaker(2021), "A Multi-Objective Constrained Robust Optimization Based on NSGA-II Algorithm," *2021 International Conference on Recent Advances in Mathematics and Informatics (ICRAMI), Tebessa, Algeria*, pp. 1-6, doi: 10.1109/ICRAMI52622.2021.9585905.

[14] K. Deb and H. Gupta, "Introducing Robustness in Multi-Objective Optimization(2006)," *Evolutionary Computation*, Vol. 14, No. 4, pp. 463-494, doi: 10.1162/evco.2006.14.4.463.

[15] Z. He, G. G. Yen and Z. Yi(2019), "Robust Multiobjective Optimization via Evolutionary Algorithms," *IEEE Transactions on Evolutionary Computation*, Vol. 23, No. 2, pp. 316-330, doi: 10.1109/TEVC.2018.2859638.

[16] Hariri-Ardebili, M.A., & Sudret, B. (2020). "Polynomial chaos expansion for uncertainty quantification of dam engineering problems", *Engineering Structures*, Vol.203, pp.109631, doi:10.1016/j.engstruct.2019.109631.

[17] Sobol, I.M., & Kucherenko, S.S. (2009). "Derivative based global sensitivity measures and their link with global sensitivity indices", Math. Comput. Simul.,Vol.79, No.10, pp. 3009-3017, doi:10.1016/j.matcom.2009.01.023.

[18] Lan, S., Li, S., & Shahbaba, B. (2021). "Scaling Up Bayesian Uncertainty Quantification for Inverse Problems Using Deep Neural Networks", SIAM/ASA Journal on Uncertainty Quantification Vol.10, No.4, pp.1684-1713, doi:10.48550/arXiv.2101.03906.